Chemistry–A European Journal
Research Article
doi.org/10.1002/chem.202300538
Chemistry Europe
European Chemical Societies Publishing
www.chemeurj.org

Special Collection

Organic-Inorganic Phenolic/POSS Hybrids Provide Highly Ordered Mesoporous Structures Templated by High Thermal Stability of PS-*b*-P4VP Diblock Copolymer

Ting-Chih Chou,[a] Wei-Cheng Chen,[a] Mohamed Gamal Mohamed,[a, b] Yen-Chi Huang,[a] and Shiao-Wei Kuo*[a, c]

Abstract: Anionic living polymerization was used to prepare a diblock copolymer of poly(styrene-*b*-4-vinyl pyridine) (PS-*b*-P4VP), and a phenolic resin with a double-decker silsesquioxane (DDSQ) cage structure was used to form a phenolic/DDSQ hybrid (PDDSQ-30 with 30 wt.% DDSQ). Strong intermolecular hydrogen bonding could be confirmed through the hydroxyl (OH) groups of PDDSQ hybrid with the pyridine group of the P4VP block in PDDSQ-30/PS-*b*-P4VP blends based on Fourier transform infrared spectroscopy analyses, where increasing PDDSQ concentrations resulted in a higher proportion of hydrogen-bonded pyridine groups. After thermal polymerization at 180 °C, the self-assembled structures of these PDDSQ/PS-*b*-P4VP blends were revealed by data from small-angle X-ray scattering (SAXS) and transmission electron microscopy (TEM), where the *d*-spacing increased with raising PDDSQ concentration. Because relatively higher thermal stability of the PDDSQ hybrid than pure phenolic resin and PS-*b*-P4VP template, we can obtain the long ranger order of mesoporous PDDSQ hybrids after removing the PS-*b*-P4VP template, which reveals the high surface area and high pore volume with cylindrical and spherical structures corresponding to the PDDSQ compositions that are rarely observed by using pure phenolic resin as the matrix and could be used in supercapacitor application.

Introduction

Diblock copolymers may create several self-assembled structures in their bulk form, such as typical spherical, cylindrical, double-gyroid, and lamellae structures, which are dependent on the volume fraction, molecular weight, and interaction parameters.[1–5] This phenomenon could be used in different applications such as photonic crystals, nanopatterns, drug delivery, and nanocomposite.[6–10] Blending homopolymer,[11,12] nanoparticle,[14,15] and organic-inorganic hybrid[16,17] into diblock copolymers to mediate the interaction parameter and volume fraction through H-bonding interaction is a facile method for the formulation of different self-assembled structures through both theoretical prediction and experimental result.[18–22] Using diblock copolymers as the template to prepare mesoporous materials with pore size from 2–50 nm with highly ordered structure and pore volume is the general approach to the phenolic or silica material.[23–26]

Therefore, the synthesis of mesoporous phenolic resin is comparable to a blend of diblock copolymer and homopolymer,[12] which is dependent on the intermolecular H-bonding interactions between the diblock copolymer template and phenolic resin,[27,28] thermal polymerization of phenolic resin in basic or acidic media, and phenolic/diblock copolymer combinations self-assembly behavior during the thermal polymerization procedure.[29] In general, highly ordered mesoporous phenolic materials are synthesized using poly(ethylene oxide) (PEO)-based diblock or triblock copolymers such as F127,[30,31] P123,[32] PEO-*b*-PS,[33,34] PEO-*b*-PLA,[35,36] PEO-*b*-PBLG,[37] and PEO-*b*-PMMA[38,39] as templates. For example, we used the thermal polymerization process to create long-range ordered mesoporous phenolic materials using PEO-*b*-PCL as templates.[40–44] Mesoporous phenolic resins with spherical, cylindric, and double gyroid structures have been obtained with mediated phenolic concentrations and volume fractions of PEO-*b*-PCL.[40–44]

However, Ikkala et al. worked the PS-*b*-P4VP as a template for the short-range order of mesoporous phenolic resin after thermal curing at 190 °C and thermal pyrolysis at 420 °C.[45,46] The disorder spherical structure was observed after pyrolysis as the PS-*b*-P4VP diblock copolymer concentration at 20 wt.%, and the BET surface area (S_{BET}) is only $<5\ m^2 g^{-1}$ and a worm-like mesoporous structure were observed before and after pyrolysis

[a] T.-C. Chou, Dr. W.-C. Chen, Prof. M. G. Mohamed, Y.-C. Huang, Prof. Dr. S.-W. Kuo
Department of Materials and Optoelectronic Science
Center for Functional Polymers and Supramolecular Materials
National Sun Yat-Sen University
Kaohsiung 804 (Taiwan)
E-mail: kuosw@faculty.nsysu.edu.tw

[b] Prof. M. G. Mohamed
Chemistry Department, Faculty of Science
Assiut University, Assiut 71515 (Egypt)

[c] Prof. Dr. S.-W. Kuo
Department of Medicinal and Applied Chemistry
Kaohsiung Medical University, Kaohsiung 807 (Taiwan)

Supporting information for this article is available on the WWW under https://doi.org/10.1002/chem.202300538

Special Collection Part of a Special Collection for "2022 Cross-strait (Hong Kong and Macao) Polymer Liquid Crystal State and Supramolecular Ordered Structure Academic Symposium."

as the diblock copolymer concentration at 30 wt.% (S_{BET} = 145 $m^2 g^{-1}$) and cylindrical structure was found at 40 wt.% diblock copolymer concentration (S_{BET} = 340 $m^2 g^{-1}$) and further isothermal treatment for 2 hr at 420 °C could obtain S_{BET} = 557 $m^2 g^{-1}$.[45–46] The mesoporous structures with short-range order were observed due to the thermal decomposition temperature of PS-*b*-P4VP being close to that of the pure phenolic resin, and thus a slight collapse of the mesoporous structure occurred.[45,46] As a consequence, the preparation of mesoporous materials templated by PS-*b*-P4VP has been generally interesting in recent years. Incorporating inorganic materials into phenolic resins could be considered a simple way to achieve this goal.[47–51]

In our previous studies,[52–58] we synthesized various compositions of double-decker silsesquioxane (DDSQ) into the phenolic resin to form phenolic/DDSQ hybrids (PDDSQ), and the thermal decomposition temperature was increased substantially with an increase in DDSQ concentration. Since the DDSQ cage structure could provide a protected inorganic layer, the thermal decomposition temperature, and char yield could be extensively improved to 532 °C and 70.4 wt.%.[54] As a result, various mesoporous phenolic PDDSQ hybrids can be prepared templated by PEO-*b*-PCL, including cylindrical, spherical, double gyroid, and even Frank-Kasper structures.[55–57] In this study, using a PS-*b*-P4VP diblock copolymer as a template, highly ordered mesoporous phenolic materials containing DDSQ hybrids was constructed.

The H-bonding interactions and self-assembled structures of the PDDSQ/PS-*b*-P4VP blends were discovered via the phenolic hydroxyl (OH) units of PDDSQ with the pyridine units of the P4VP block segment by FTIR, TEM, and SAXS investigations. Following the removal of the PS-*b*-P4VP template, SAXS, TEM, and N_2 adsorption/desorption isotherms were utilized to analyze the surface area, pore size, and self-assembled mesoporous structures of the mesoporous phenolic/DDSQ hybrids.

Experimental Section

Materials

4-Vinylpyridine (99%) and styrene (99%) monomers were purchased from Aldrich. Scheme 1(a) displayed the synthesis of PS_{263}-*b*-$P4VP_{106}$ diblock copolymer (PDI = 1.04) by sequential anionic living polymerization described elsewhere.[59] Phenyltrimethoxysilane, methyl dichlorosilane, sodium hydroxide (NaOH), CH_2O, nadic anhydride, paraformaldehyde (CH_2O), phenol, and 4-aminophenol were acquired from Sigma-Aldrich. Phenolic/DDSQ (PDDSQ) hybrid with 30 wt.% DDSQ weight fraction was synthesized through phenol and DDSQ–4OH, which was described previously as shown in Scheme 1(b).[54–56]

The preparation of PPDSQ/PS-b-P4VP blends and mesoporous PDDSQ hybrids

PS-*b*-P4VP with various concentrations of PDDSQ-30 were separately stirred in THF solution at 25 °C for 24 h, and these solutions were poured into an aluminum plate, sealed with aluminum foil, and slowly evaporated based on the evaporation-induced self-assembly mechanism at 40 °C for 2 days. After drying out the THF solution, the samples were placed in an oven for thermal polymer-

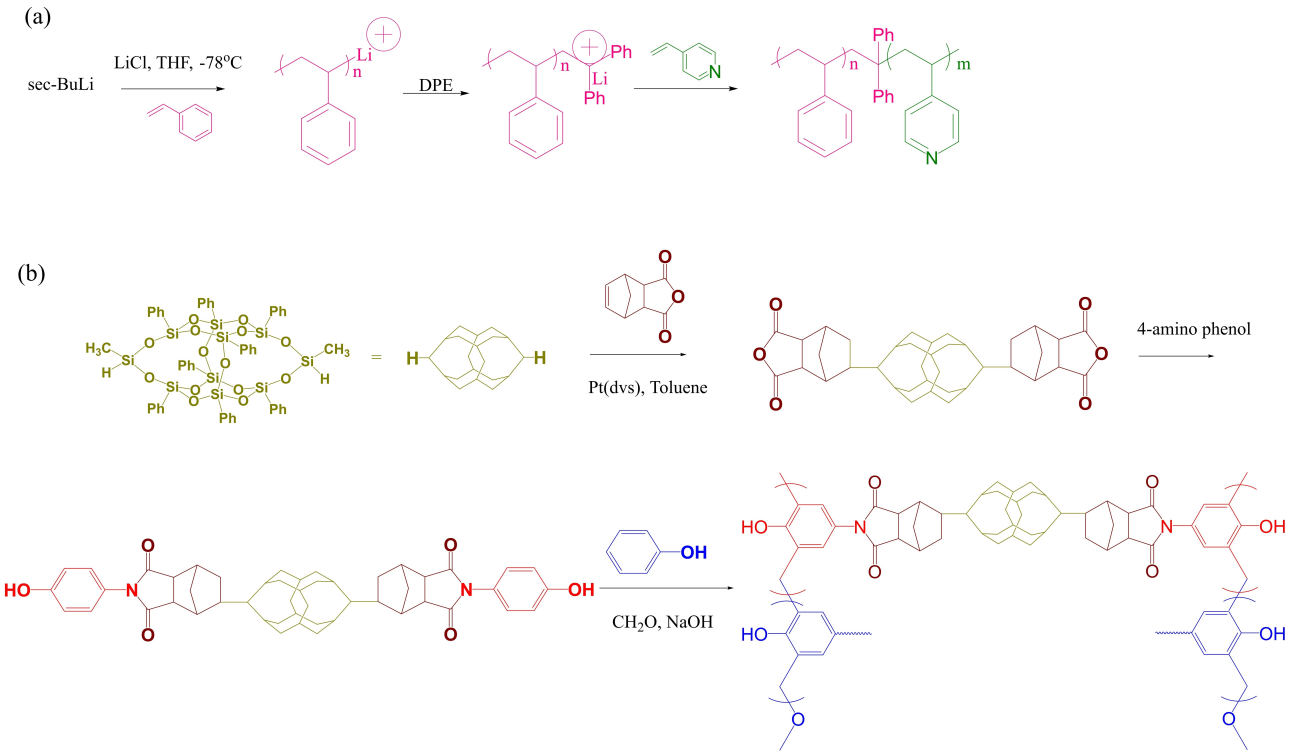

Scheme 1. (a) The synthesis of PS-*b*-P4VP by anionic living polymerization and (b) the synthesis of phenolic/DDSQ hybrids through DDSQ, hydrosilylation with nadic anhydride, 4-amino phenol to form DDSQ-4OH and then copolymerization with phenol and CH_2O.

ization at 180 °C for 24 h, and self-assembled structures of the PDDSQ/PS-*b*-P4VP hybrids were achieved. Mesoporous PDDSQ hybrids were formed by thermal pyrolysis at 450 °C for 10 h to remove the PS-*b*-P4VP diblock copolymer, as expected.

Results and Discussion

FTIR, SAXS and TEM analyses of PDDSQ/PS-b-P4VP blends

In our previous reports, the intermolecular H-bonding between the pyridine groups of P4VP and the phenolic OH groups were discussed and investigated with a strong inter-association equilibrium constant ($K_A = 1200$).[29] Figure 1 shows the FITR profiles of PDDSQ-30/PS-*b*-P4VP blends with various compositions recorded at room temperature. Pure PDDSQ-30 hybrid displays two major absorptions at 3370 and 3560 cm^{-1} for its OH units, corresponding to self-association hydrogen bonding and free OH groups, respectively.[54] Generally, the self-association OH units of the PDDSQ-30 hybrid are shifted to a lower wavenumber from 3370 to 3220 cm^{-1}, and as the concentration of PS-*b*-P4VP is increased, the intensity of the free OH groups decreases, as displayed in Figure 1(a), indicating the formation of strong intermolecular H-bonding between pyridine units and phenolic OH.[60] Figure 1(b) shows the FTIR patterns for the pyridine groups of the P4VP block segment ranging from 1020 to 975 cm^{-1} of different PDDSQ-30/PS-*b*-P4VP blends. A free pyridyl ring was observed at 993 cm^{-1} for the P4VP segment, and after blending with the PDDSQ hybrid, a distinct absorption peak at 1003 cm^{-1} was noticed caused by the intermolecular hydrogen-bonded phenolic OH with pyridine units, and upon rising PDDSQ concentration, there was a noticeable rise in the percentage of hydrogen-bonded pyridine rings, as expected (Scheme 2).[60]

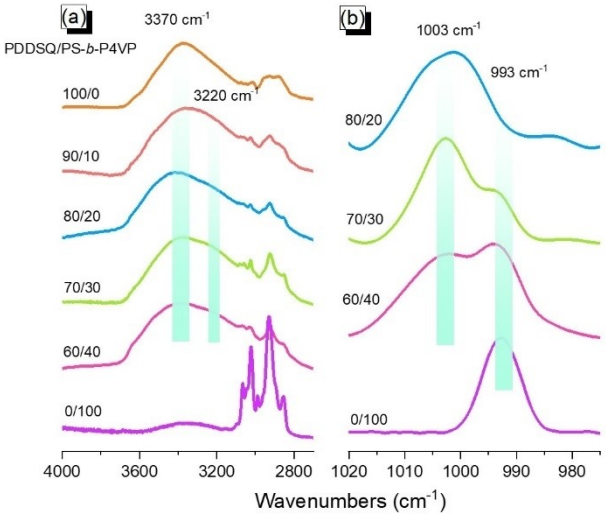

Figure 1. FTIR spectroscopy analyses of PDDSQ-30/PS-*b*-P4VP blends of (a) OH stretching and (b) pyridine units.

The SAXS patterns of the different PDDSQ-30/PS-*b*-P4VP blends obtained at room temperature are shown in Figure 2(a). The double gyroid structure of pure PS-*b*-P4VP block copolymer exhibits a high order with peak ratios of $\sqrt{6}:\sqrt{8}:\sqrt{20}:\sqrt{26}:\sqrt{54}$, where the PS block segment's volume fraction is 0.67, and the first peak appears at 0.142 nm^{-1} due to $\sqrt{6}q^*$ ($d = 44.22$ nm), which is verified by it corresponding TEM image shown in Figure 2(b) from the [2 1 1] direction.[59] At 60 wt.% PDDSQ-30, the SAXS pattern displayed a cylindrical shape in a long-range order with a peak ratio of $1:\sqrt{4}:\sqrt{7}:\sqrt{9}$, and the first q^* peak was located at 0.177 nm^{-1} ($d = 35.48$ nm), as seen by the TEM pictures in Figure 2(c). Here, we did not use any staining agent, and thus, the PDDSQ domain appears as a dark region, and an area that is white denotes the PS or P4VP domain. The bicontinuous phase of the PS domain is observed in Figure 2(b); however, it was transformed into a dispersed cylindrical phase after blending with 60 wt.% of PDDSQ-30 (Figure 2(c)).

Upon further increasing the PDDSQ-30 at 70 wt.%, The SAXS pattern further demonstrated the cylindrical structure's long-range order, with the peak ratio of $1:\sqrt{3}:\sqrt{4}:\sqrt{7}$, and the first q^* peak was located at 0.181 nm^{-1} ($d = 34.69$ nm), as revealed by the TEM image in Figure 2(d). Similarly, the SAXS pattern exhibited a cylindrical structure for 80 wt.% PDDSQ-30 with a

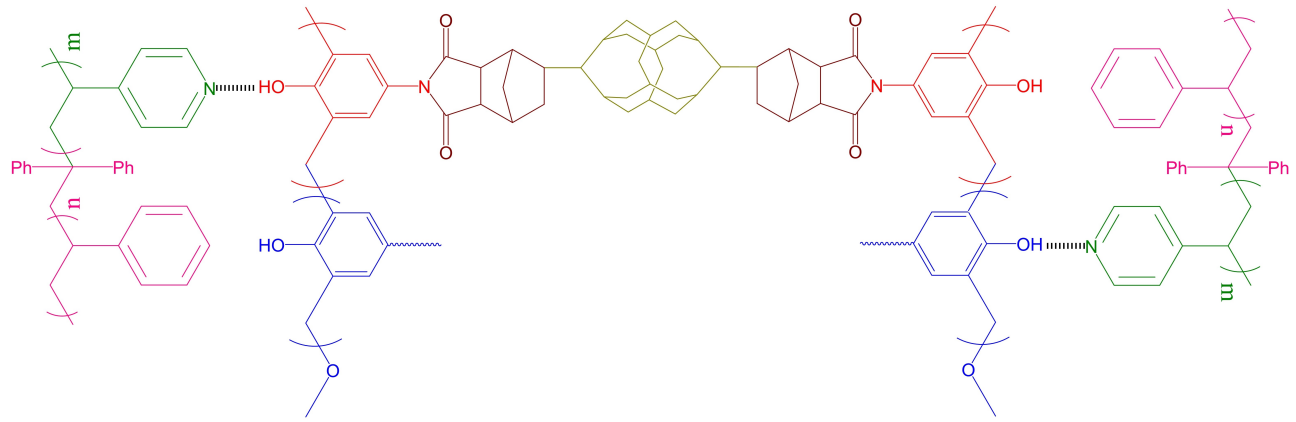

Scheme 2. The intermolecular H-bonding interaction of PDDSQ-30/PS-*b*-P4VP blends through the phenolic OH units of PDDSQ hybrids and the pyridine unit of the P4VP block segment.

Research Article
doi.org/10.1002/chem.202300538

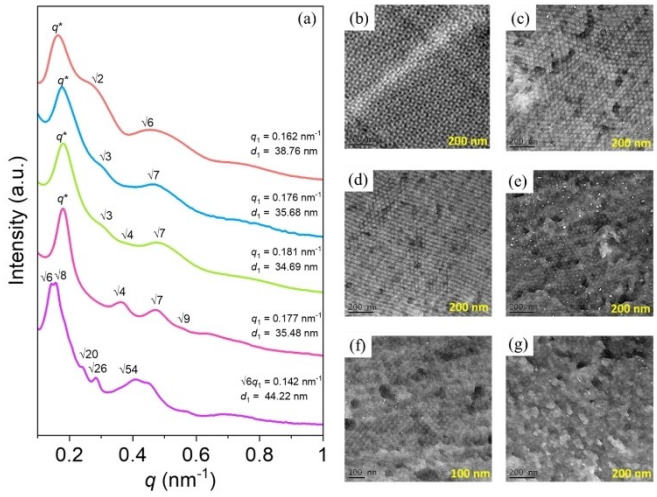

Figure 2. (a) SAXS analyses of PDDSQ-30/PS-*b*-P4VP blends [PS-b-P4VP (violet), 60/40 (pink), 70/30 (green), 80/20 (bright blue), 90/10 (red)] and their corresponding TEM images of PDDSQ-30/PS-*b*-P4VP blends = (b) pure PS-*b*-P4VP, (c) 60/40, (d) 70/30, (e) 80/20, and (f, g) 90/10.

peak ratio of 1:$\sqrt{3}$:$\sqrt{7}$, and the first q^* peak was located at 0.176 nm^{-1} (d = 35.68 nm), as confirmed by the TEM image in Figure 2(e). Upon increasing the PDDSQ-30 at 90 wt.%, the SAXS pattern exhibited a spherical structure with peak ratios of 1:$\sqrt{2}$:$\sqrt{6}$, and the first peak (q^*) was located at 0.162 nm^{-1} (d = 38.76 nm), as investigated by the TEM images in Figures 2(f) and 2(g), which display the short range of spherical micelle structure by TEM data, due to the order-order self-assembled transition by wet-brush behavior[27] occurred in this PDDSQ/PS-*b*-P4VP blend from double gyroid, cylindrical, and spherical structures upon increasing the PDDSQ hybrid concentration as shown in Scheme 3(a). Because the OH units of the PDDSQ hybrids have strong H-bonding interactions with the P4VP block segment from the miscible PDDSQ/P4VP domain, various micro-phase-separation morphologies of the PS domains were formed in these PDDSQ/PS-*b*-P4VP systems.

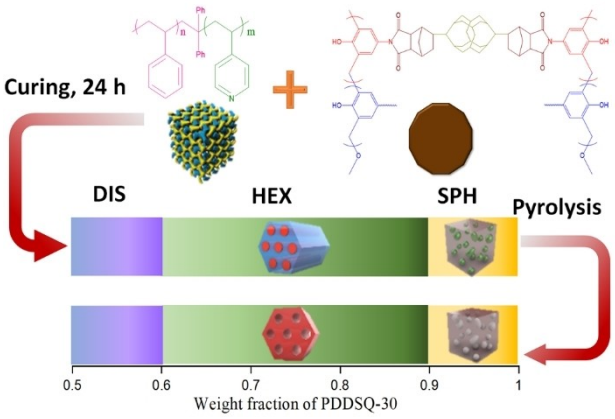

Scheme 3. The chemical and self-assembly structures of (a) PDDSQ/PS-*b*-P4VP blend after thermal curing and (b) mesoporous PDDSQ after removal template.

DSC and SAXS analyses of PDDSQ/PS-b-P4VP blends during thermal polymerization

DSC thermal analysis is a convenient characterization method for gaining an understanding of the thermal and miscibility characteristics of polymer blend systems. Figure 3 shows the first-run DSC thermograms of the various PDDSQ-30/PS-*b*-P4VP blend compositions. Pure PS-*b*-P4VP shows two T_g values, comparable to the T_g values of the PS and P4VP block segments at approximately 108 °C and 152 °C, respectively.[59] After blending with the PDDSQ-30 hybrid, the PS block segment's T_g value increased from 108 to 115 °C upon increasing the PDDSQ-30 concentration in the blend system. This result is due to the strong H-bonding interaction in the PDDSQ/P4VP miscible domain (relatively high T_g value), which could confine the mobility of the PS block segment. Furthermore, the thermal polymerization temperature increased from 182 to 203 °C with increasing PDDSQ-30 concentration in the blend system.

To comprehend the self-assembled structures produced by thermal polymerization of the PDDSQ-30/PS-*b*-P4VP system, the SAXS patterns of each blend composition were recorded at various temperatures, as shown in Figure 4. We observed that the first peaks were moved to lower q values for the compositions with cylindrical structures, such as PDDSQ-30/PS-*b*-P4VP = 60/40, 70/30, and 80/20 blend systems, with an increase in the thermal curing temperature, as expected due to thermal expansion. For example, the q^* = 0.181 nm^{-1}, d = 34.69 nm at 30 °C and q^* = 0.163 nm^{-1}, d = 38.52 nm at 180 °C

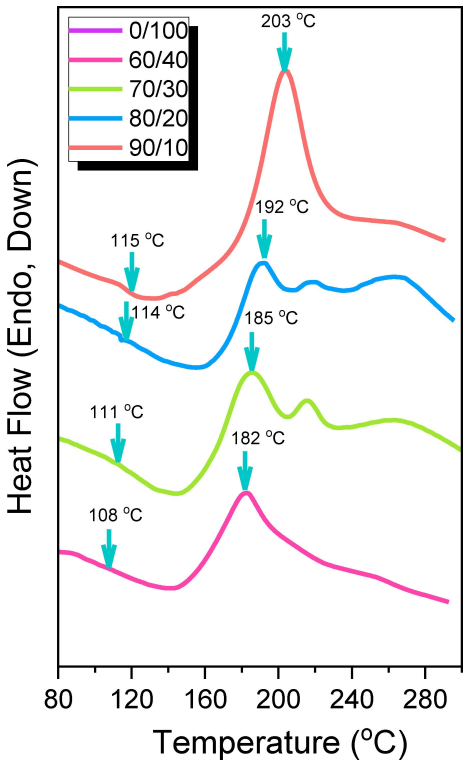

Figure 3. DSC thermograms of various PDDSQ-30/PS-*b*-P4VP blends during the first heating scan.

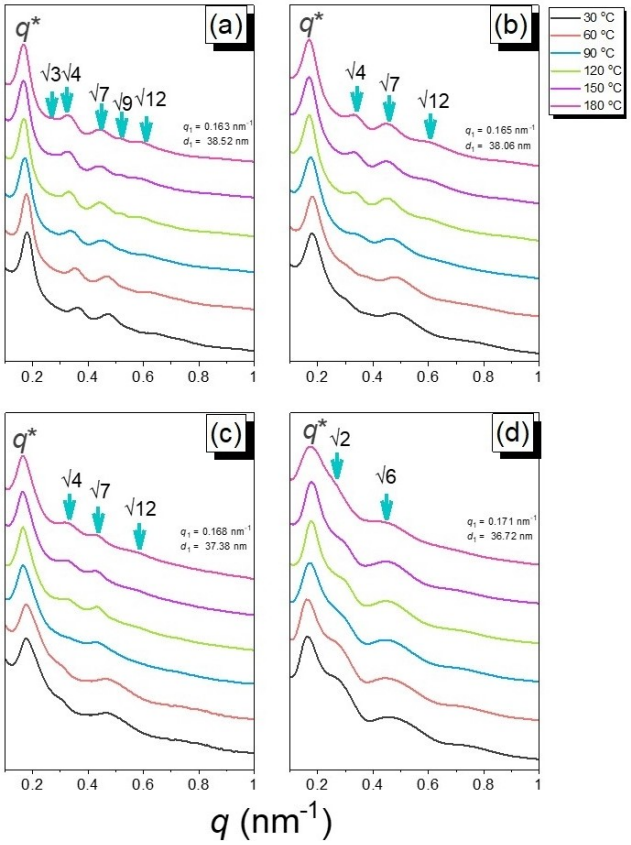

Figure 4. SAXS patterns recorded at various thermal polymerization temperatures of PDDSQ-30/PS-*b*-P4VP blends = (a) 60/40, (b) 70/30, (c) 80/20, and (d) 90/10.

for PDDSQ-30/PS-*b*-P4VP = 60/40 (Figure 4(a)), $q^* = 0.177\ nm^{-1}$, $d = 35.48$ nm at 30 °C and $q^* = 0.165\ nm^{-1}$, $d = 38.06$ nm at 180 °C for PDDSQ-30/PS-*b*-P4VP = 70/30 (Figure 4(b)), and $q^* = 0.176\ nm^{-1}$, $d = 35.68$ nm at 30 °C and $q^* = 0.168\ nm^{-1}$, $d = 37.38$ nm at 180 °C for PDDSQ-30/PS-*b*-P4VP = 80/20 (Figure 4(c)) blend system were observed. Clearly, the self-assembled cylindrical structure becomes much more ordered with increasing thermal curing temperature; for example, the $\sqrt{4}$ scattering peak becomes obvious and sharp for the PDDSQ-30/PS-*b*-P4VP = 70/30 and 80/20 blend systems. This phenomenon could be explained by the increased thermal curing temperature, which enhances the reaction-induced microphase separation behavior.[29] During thermal polymerization, the entropy of mixing generally decreases substantially because of the significantly increasing molecular weight of PDDSQ, which induces unfavorable Gibbs free energy and subsequently creates highly organized self-assembling structures. In addition, the thermal expansion decreased with increasing PDDSQ concentration, indicating a rigid PDDSQ/P4VP miscible domain that is much more difficult to expand thermally. As a result, the shrinkage of spherical structure *d*-spacing of $q^* = 0.162\ nm^{-1}$, $d = 38.76$ nm at 30 °C and $q^* = 0.171\ nm^{-1}$, $d = 36.72$ nm at 180 °C were observed for PDDSQ-30/PS-*b*-P4VP = 90/10 blend (Figure 4(d)) at relative higher PDDSQ-30 content and this result may also as the thermal curing temperature rises, the order-order changes from a spherical to a cylindrical structure.

Mesoporous PDDSQ hybrids templated by PS-b-P4VP diblock copolymer

To ensure the formation of mesopores templated by the high thermal stability of the PS-*b*-P4VP, TGA analyses of PS-*b*-P4VP diblock copolymer and pure PDDSQ-30 are displayed in Figure 5(a); a weight loss of 10 and 50 wt.% at 351 °C and 412 °C for pure PS-*b*-P4VP and a weight loss of 10 wt.% at 533 °C and a char yield of 70 wt.% for pure PDDSQ were observed.[54] To confirm the complete removal of the PS-*b*-P4VP, we chose 450 °C to remove the PS-*b*-P4VP by pyrolysis under a nitrogen atmosphere, and it still maintained the framework of the PDDSQ-30 hybrid. Figure 5(b) shows the TGA results of all mesoporous PDDSQ hybrids after PS-*b*-P4VP diblock copolymer template removal by thermal pyrolysis at 450 °C for 10 h. Clearly, the T_{d10} values and char yield of these mesoporous PDDSQ hybrids increased to 577–604 °C and 79.6–81.1 wt.%, respectively. Clearly, the different amounts of PS-*b*-P4VP diblock copolymer template showed similar char yields for these mesoporous PDDSQ hybrids, also suggesting complete template removal by thermal pyrolysis at 450 °C. Additionally, slight thermal decompositions (2–3 wt.%) ranging from 50 to 150 °C for all mesoporous PDDSQ hybrids generally occurred owing to the moisture absorption of porous materials, also indicating the formation of a mesoporous structure, as expected.[55–56] Thermal calcination was used to remove the PS-*b*-P4VP diblock copolymer template after thermal polymerization and to obtain mesoporous PDDSQ hybrids.

Selected SAXS patterns measured before and after thermal pyrolysis were used for comparison, as shown in Figure 6. After thermal pyrolysis of both PDDSQ-30/PS-*b*-P4VP = 80/20 and 70/30, the first peaks were shifted to a higher q^* value,

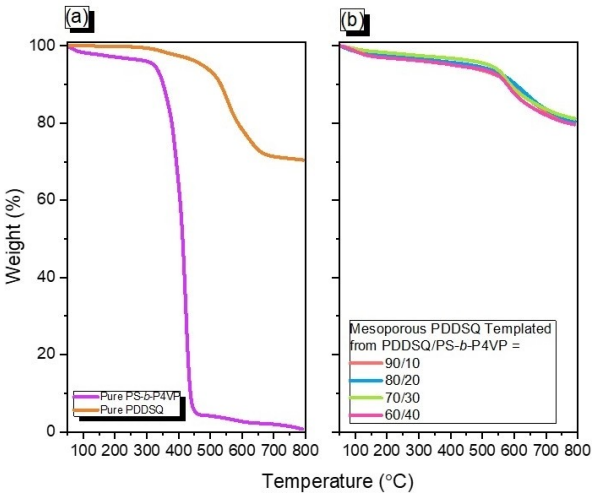

Figure 5. TGA data of (a) pure PS-*b*-P4VP and pure PDDSQ hybrid and (b) various mesoporous PDDSQ templated from various PS-*b*-P4VP diblock copolymer template compositions.

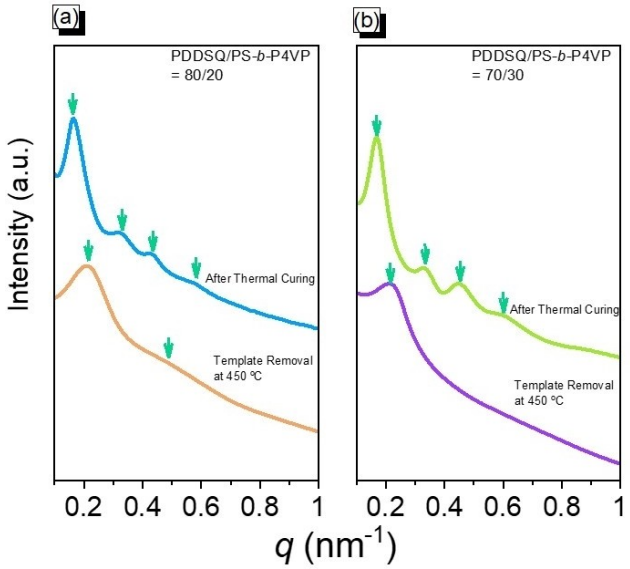

Figure 6. SAXS patterns analyses before and after thermal pyrolysis of PDDSQ-30/PS-*b*-P4VP blends of (a) 80/20 and (b) 70/30.

indicating shrinkage of the PDDSQ structure during thermal calcination, resulting in a decrease in the mesoporous domain size, as expected.[55–56]

Figure 7 shows the SAXS and TEM studies of the mesoporous PDDSQ hybrids derived from the PS-*b*-P4VP diblock copolymer at different PDDSQ-30 concentrations. The single wide scattering peak for the mesoporous PDDSQ hybrid from PDDSQ-30/PS-*b*-P4VP = 90/10 [Figure 7(a)], demonstrates the short-range order of the spherical micelle structure [Figure 7(e)]. The SAXS pattern of the mesoporous PDDSQ hybrid with peak ratios of $1:\sqrt{3}:\sqrt{4}:\sqrt{7}$ in Figure 7(b) suggests the long-range order of the cylindrical structure, which is supported by the TEM picture in Figure 7(f). This result is quite different from that of pure phenolic templated by PS-*b*-P4VP diblock copolymer during isothermal treatment for 2 h at 420 °C.[45–46] A slight collapse of the cylindrical mesopores was observed because of the relatively lower thermal stability of pure phenolic compared with our PDDSQ hybrid,[54] which is an isothermal treatment for 10 h at 450 °C. Further increase in the PS-*b*-P4VP contents, Figures 7(c) and 7(d) display the short-range order of mesoporous cylindrical structures with peak ratios of $1:\sqrt{3}$ or $1:\sqrt{7}$, as confirmed in Figures 7(g) and 7(h) by TEM analyses. Furthermore, we can observe that the first peaks of mesoporous PDDSQ hybrid were shifted to the lower q value upon increasing PS-*b*-P4VP diblock copolymer template concentrations from $q^* = 0.218\ nm^{-1}$, $d = 28.80$ nm from PDDSQ-30/PS-*b*-P4VP = 90/10 and $q^* = 0.199\ nm^{-1}$, $d = 31.55$ nm from PDDSQ-30/PS-*b*-P4VP = 60/40 blend. The relatively higher PDDSQ-30 hybrid could explain this phenomenon; a relatively higher fraction of hydrogen-bonded pyridine units could be observed, as shown in Figure 1(b), which resulted in an increase in the thickness of the PDDSQ/P4VP domain and a decrease in the microphase separation domain size from the PS segment and the self-assembled structure of mesoporous PDDSQ hybrids was summarized in Scheme 3(b).

Mesoporous PDDSQ hybrid nitrogen adsorption/desorption isotherms recorded at 77 K and templated from PDDSQ-30/PS-*b*-P4VP = 80/20 and PDDSQ-30/PS-*b*-P4VP = 70/30 are shown in Figure 8. According to the traditional type IV graphs of the mesoporous PDDSQ hybrid formed from PDDSQ-30/PS-*b*-P4VP = 80/20, there was a sharp capillary condensation step at the P/P_0 value between 0.85 and 0.95, and H_1 hysteresis loops appeared in the relative pressure range between 0.4 and 0.9, indicating the existence of cylindrical mesoporous shapes, as shown in Figure 8(a). According to the Harkins and Jura model, the average pore size based on the Harkins and Jura model was ca. 28.6 nm in Figure 8(c), which is much larger than that of the PEO-based diblock copolymer templates with a similar degree of polymerization. Furthermore, Figure 8(b) also provides the typical type IV curve of the mesoporous PDDSQ hybrid formed

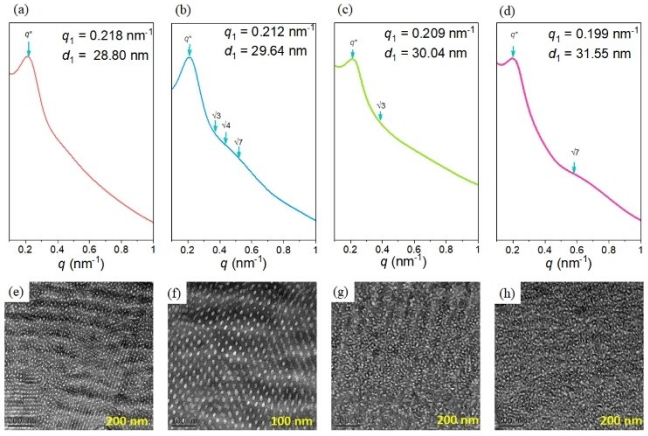

Figure 7. (a–d) SAXS patterns and (e–h) TEM images of mesoporous PDDSQ hybrids formed from PDDSQ-30/PS-*b*-P4VP blends of (a, e) 90/10, (b, f) 80/20, (c, g) 70/30 and (d, h) 60/40.

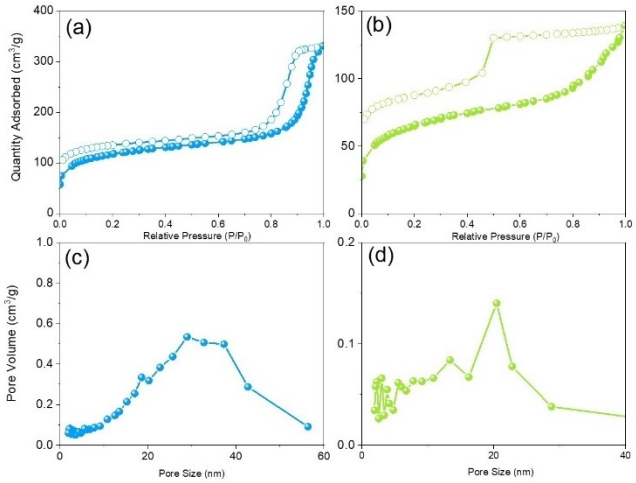

Figure 8. (a–b) nitrogen adsorption/desorption isotherm and (c–d) pore size distribution of mesoporous PDDSQ hybrids formed from PDDSQ-30/PS-*b*-P4VP blends of (a, c) 80/20 and (b, d) 70/30.

from PDDSQ-30/PS-*b*-P4VP = 70/30, H_2 hysteresis loop (at P/P_0 value from 0.4 to 0.9), and sharp capillary condensation step (at P/P_0 value from 0.85 to 0.95), and also suggesting a pore cylindrical with a cage mesoporous structure with an average pore size of ca. 20.1 nm as shown in Figure 8(d). The BET analyses of these two mesoporous PDDSQ hybrids indicate a high BET surface area (384 and 218 m^2/g), pore volume, and mesoporous surface area, which is already higher than the mesoporous phenolic resin templated from PEO-*b*-PCL (only ranging from 60 to 140 m^2/g)[38] and a few PS-*b*-P4VP diblock copolymer.[47–51]

The high surface area, high pore volume, and large pore size of these mesoporous PDDSQ hybrids could be used in gas capture and energy storage applications, as discussed in our previous works.[54,55] Two peaks at 1321 and 1586 cm^{-1} in the Raman profile [Figure S1] correspond to D and G Bands in mesoporous PDDSQ/carbon hybrids.

CV and GCD analyses of mesoporous PDDSQ/carbon hybrids

The cylindrical mesoporous PDDSQ/carbon hybrids from PDDSQ-30/PS-*b*-P4VP = 70/30 mixtures could exhibit large pores, high surface areas, and no structural collapse after the activation process at 900 °C as expected, suggesting that they have good prospects for use as active electrode materials for electric double-layer capacitors (EDLC). We tested the electrochemical properties (cyclic voltammetry (CV) and galvanostatic charge/discharge (GCD) analyses) of the mesoporous PDDSQ/carbon hybrid materials from PDDSQ-30/PS-*b*-P4VP = 70/30 mixtures as working electrodes in a three-electrode cell system with 1 M aqueous KOH solution as the electrolyte and Hg/HgO as the reference electrode. As seen in Figure 9(a), the cyclic voltammetry patterns at different scan rates (5–200 mV s^{-1}) of the cylindrical mesoporous PDDSQ/carbon hybrid materials displayed a rectangular shape because of the presence of heteroatom doping in the mesoporous PDDSQ/carbon hybrid materials.[61–65] These results indicate that this material exhibits the behavior of EDLC supercapacitors and pseudocapacitance (PC).[61–68] Additionally, the cylindrical mesoporous PDDSQ/carbon hybrid materials had a uniform triangular charge-discharge shape (Figure 9(b)), which is a common characteristic of supercapacitive materials with constant charge and discharge. Based on the GCD curve, the specific capacitance can be calculated using the formula ($Cs = (I \times \Delta t)/(m \times \Delta V)$. The specific capacitances of the mesoporous PDDSQ/carbon hybrid materials at various current densities [Figure 9(c)] were 966, 613, 496, 469, 415, 388, 350, 316, and 279 F g^{-1} at 0.5, 1, 2, 3, 5, 7, 10, 15, and 20 A g^{-1}, respectively. The excellent performance of mesoporous PDDSQ/carbon hybrid materials in energy storage applications is due to their high nitrogen content, pore size, surface area, and pore volume. These factors are also beneficial for facilitating the entry of electrolytes into the electrode surface and improving the rate capability. Figure 9(d) shows the capacity retention of the mesoporous PDDSQ/carbon hybrid material recorded after 2000 cycles. As shown in Figure 9(d), the capacitance retention of this material was 94% after 2000 cycles. Table S1 summarizes the capacitance performance of cylindrical mesoporous PDDSQ/carbon hybrid materials with other reported materials. The energy density of mesoporous PDDSQ/carbon hybrid materials was calculated to be 134 Wh Kg^{-1}, as shown in Figure S2.

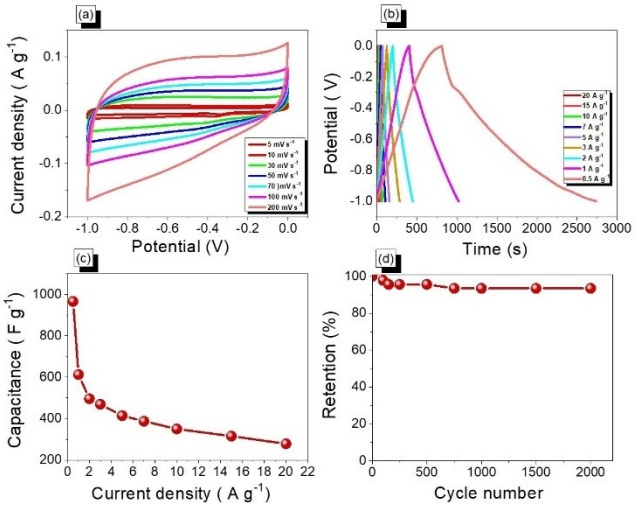

Figure 9. CV curves conducted in 6 M KOH for various scan rates of (a) GCD profile recorded at numerous current densities of mesoporous PDDSQ/carbon hybrid materials (b) Specific capacitance graph (c) and Cycling performance derived from PDDSQ-30/PS-*b*-P4VP = 70/30 mixtures (d).

Conclusion

The PS-*b*-P4VP as the template and the organic-inorganic phenolic/DDSQ hybrid as the matrix was used in this study, which could form strong intermolecular H-bonding interactions between the OH units of PDDSQ and the pyridine moieties of the P4VP block segment, based on FTIR analyses. The self-assembled structure in the PDDSQ/PS-*b*-P4VP blends could be understood using SAXS and TEM investigations, and the *d*-spacing increased when the PDDSQ concentrations were raised, corresponding to an increase in the proportion of H-bonded pyridine units of the P4VP block segment after thermal treatments at 180 °C with the wet-brush behavior from double gyroid, cylindrical, and spherical structures. After removing the PS-*b*-P4VP diblock copolymer template, the long-range order of the mesoporous PDDSQ hybrids was simply produced due to the excellent thermal stability of the PDDSQ hybrids. The electrochemical data revealed that the mesoporous PDDSQ/carbon hybrid materials exhibited good rate capabilities, a capacitance of up to 966 F g^{-1}, and no decrease in efficiency after 2000 cycles. This research offers a method to improve the material's ability and made from mesoporous PDDSQ hybrids, creating a new supply of electroactive materials.

Acknowledgements

This study was supported financially by the Ministry of Science and Technology, Taiwan, under contracts NSTC 111-2222-E-110-004 and 109-2221-E-110-067-MY3.

Conflict of Interest

The authors declare no conflict of interest.

Data Availability Statement

Research data are not shared.

Keywords: block copolymers · mesoporous materials supercapacitors · supramolecular interaction · self-assembled structures

[1] C. Cummins, R. Lundy, J. J. Walsh, V. Ponsinet, G. Fleury, M. A. Morris, *Nano Today* **2020**, *35*, 100936.
[2] T. Liu, G. Liu, *J. Mater. Chem. A* **2019**, *7*, 23476.
[3] M. Karayianni, S. Pispas, *J. Polym. Sci.* **2021**, *59*, 1874–1898.
[4] Y. Shao, D. Han, Y. Tao, F. Feng, G. Han, B. Hou, H. Liu, S. Yang, Q. Fu, W. B. Zhang, *ACS Cent. Sci.* **2023**, *9*, 289–299.
[5] L. Guo, Y. Wang, M. Steinhart, *Chem. Soc. Rev.* **2021**, *50*, 6333–6348.
[6] E. L. Lin, W. L. Hsu, Y. W. Chiang, *ACS Nano* **2018**, *12*, 485–493.
[7] A. A. Kulkami, G. S. Doerk, *ACS Appl. Mater. Interfaces* **2022**, *14*, 27466–27475.
[8] A. M. Jazani, J. K. Oh, *Polym. Chem.* **2020**, *11*, 2934–2954.
[9] S. Liang, M. Zhang, G. M. Biesold, W. Choi, Y. He, Z. Li, D. Shen, Z. Lin, *Adv. Mater.* **2021**, *33*, 2005888.
[10] Y. Shao, B. Hou, W. Li, X, Yan, X. Wang, Y. Xu, Q. Dong, W. Li, J. He, W. B. Zhang, *Macromolecules* **2023**, *56*, 1562–1571.
[11] H. Takagi, K. Yamamoto, *Macromolecules* **2019**, *52*, 2007–2014.
[12] S. W. Kuo, *Polym. Int.* **2022**, *71*, 393–410.
[13] J. Wang, L. Liu, G. Yan, Y. Li, Y. Gao, Y. Tian, L. Jiang, *ACS Appl. Mater. Interfaces* **2021**, *16*, 14507–14517.
[14] W. J. Zhang, C. Y. Hong, C. Y. Pan, *Macromol. Rapid Commun.* **2019**, *40*, 1800279.
[15] N. Yan, X. Liu, J. Zhu, Y. Zhu, W. Jiang, *ACS Nano* **2019**, *13*, 6638–6646.
[16] A. Pourjavadi, S. Rahemipoor, M. Kohestanian, *Compos. Sci. Technol.* **2020**, *188*, 107951.
[17] S. Ayaia, K. C. Bentz, S. M. Cohen, *Chem. Sci.* **2019**, *10*, 1746–1753.
[18] B. Vorselaars, R. K. W. Spencer, M. W. Matsen, *Phys. Rev. Lett.* **2020**, *125*, 117801.
[19] J. Xie, A. C. Shi, *Giant* **2021**, *5*, 100043.
[20] J. Diaz, M. Pinna, A. V. Zvelindovsky, I. Pagonabarraga, *Macromolecules* **2019**, *52*, 8285–8294.
[21] S. W. Hsu, T. Xu, *Macromolecules* **2019**, *52*, 2833–2842.
[22] G. K. Sethi, H. Y. Jung, W. S. Loo, S. Sawhney, M. J. Park, N. P. Balsara, I. Vilaluenga, *Macromolecules* **2019**, *52*, 3165–3175.
[23] D. Zhao, J. Feng, Q. Huo, N. Melosh, G. H. Fredrickson, B. F. Chmelka, G. D. Stucky, *Science* **1998**, *279*, 548–552.
[24] C. Li, Q. Li, Y. V. Kaneti, D. Hou, Y. Yamauchi, Y. Mai, *Chem. Soc. Rev.* **2020**, *49*, 4681–4736.
[25] Y. Deng, J. Wei, Z. Sun, D. Zhao, *Chem. Soc. Rev.* **2013**, *42*, 4054–4070.
[26] K. Lan, D. Zhao, *Nano Lett.* **2022**, *22*, 3177–3179.
[27] H. Kosonen, J. Ruokolainen, P. Nyholm, O. Ikkala, *Polymer* **2001**, *42*, 9481–9486.
[28] C. Liang, S. Dai, *J. Am. Chem.* **2006**, *128*, 5316–5317.
[29] S. W. Kuo, *Hydrogen Bonding in Polymer Materials*, Wiley-VCH, Weinheim (**2018**).
[30] Y. Huang, J. Yang, H. Cai, Y. Zhai, D. Feng, Y. Deng, B. Tu, D. Zhao, *J. Mater. Chem.* **2009**, *19*, 6536–6541.
[31] W. C. Chu, S. F. Chiang, J. G. Li, S. W. Kuo, *Materials* **2013**, *6*, 5077–5093.
[32] L. Liu, F. Y. Wang, G. S. Shao, T. Y. Ma, Z. Y. Yuan, *Carbon* **2010**, *48*, 2660–2664.
[33] Y. Deng, T. Yu, Y. Wan, Y. Shi, Y. Meng, D. Gu, L. Zhang, Y. Huang, C. Liu, X. Wu, D. Zhao, *J. Am. Chem.* **2007**, *129*, 1690–1697.
[34] D. Hu, Z. Xu, K. Zeng, S. Zheng, *Macromolecules* **2010**, *43*, 2960–2969.
[35] J. G. Li, P. Y. Lee, M. M. M. Ahmed, M. G. Mohamed, S. W. Kuo, *Macromol. Chem. Phys.* **2020**, *221*, 200040.
[36] M. G. Mohamed, W. S. Hung, A. F. M. EL-Mahdy, M. M. M. Ahmed, L. Dai, T. Chen, S. W. Kuo, *Polymer* **2020**, *12*, 1193.
[37] A. F. M. EL-Mahdy, T. C. Yu, M. G. Mohamed, S. W. Kuo, *Macromolecules* **2021**, *54*, 1030–1042.
[38] Y. Deng, C. Liu, D. Gu, T. Yu, B. Tu, D. Zhao, *J. Mater. Chem.* **2008**, *18*, 91–97.
[39] J. Wei, Y. Deng, J. Zhang, Z. Su, B. Tu, D. Zhao, *Solid State Sci.* **2011**, *13*, 784–792.
[40] J. G. Li, Y. D. Lin, S. W. Kuo, *Macromolecules* **2011**, *44*, 9295–9309.
[41] J. G. Li, W. C. Chu, U. S. Jeng, S. W. Kuo, *Macromol. Chem. Phys.* **2013**, *214*, 2115–2123.
[42] W. C. Chu, B. P. Bastakoti, Y. V. Kaneti, J. G. Li, H. R. Alamri, Z. A. Alothman, Y. Yamauchi, S. W. Kuo, *Chem. Eur. J.* **2017**, *23*, 13734–13741.
[43] J. G. Li, C. Y. Chung, S. W. Kuo, *J. Mater. Chem.* **2012**, *22*, 18583–18595.
[44] J. G. Li, Y. F. Ho, Mahmoud, M. M. Ahmed, H. C. Liang, S. W. Kuo, *Chem. Eur. J.* **2019**, *25*, 10456–10463.
[45] H. Kosonen, S. Valkama, A. Nykanen, M. Toivanen, G. ten-Brinke, J. Ruokolainen, O. Ikkala, *Adv. Mater.* **2006**, *18*, 201–205.
[46] S. Valkama, A. Nykanen, H. Kosonen, R. Ramani, F. Tuomisto, P. Engelhardt, G. ten-Brinke, O. Ikkala, J. Ruokolainen, *Adv. Funct. Mater.* **2007**, *17*, 183–190.
[47] H. Li, H. Shen, C. Pei, S. Chen, Y. Wan, *ChemCatChem* **2019**, *11*, 3882–3291.
[48] S. Yin, W. Cao, Q. Ji, Y. Cheng, L. Song, N. Li, C. L. Weindl, M. Schwartzkopf, S. V. Roth, P. M. Buschbaum, *Adv. Mater. Interfaces* **2021**, *8*, 2100141.
[49] K. Wang, S. Xia, W. Cao, N. Hohn, S. Grott, L. P. Kreuzer, M. Schwartzkopf, S. V. Roth, P. M. Buschbaum, *ACS Appl. Nano Mater.* **2018**, *1*, 7139–7148.
[50] H. Ouyang, C. Fang, Z. Xu, L. Li, G. Xiao, *Nanoscale* **2022**, *14*, 11298–11304.
[51] L. Liu, X. Yang, Y. Xie, H. Liu, X. Zhou, X. Xiao, Y. Ren, Z. Ma, X. Cheng, Y. Deng, D. Zhao, *Adv. Mater.* **2020**, *32*, 1906653.
[52] Y. T. Liao, Y. C. Lin, S. W. Kuo, *Macromolecules* **2017**, *50*, 5739–5747.
[53] W. C. Chen, S. W. Kuo, *Macromolecules* **2018**, *51*, 9602–9612.
[54] W. C. Chen, Y. T. Liu, S. W. Kuo, *Polymer* **2020**, *12*, 2151.
[55] W. C. Chen, Y. Z. Liu, S. W. Kuo, *Macromol. Rapid Commun.* **2021**, *42*, 2100302.
[56] Y. C. Huang, W. C. Chen, S. W. Kuo, *Macromolecules* **2022**, *55*, 8918–8930.
[57] M. G. Mohamed, S. W. Kuo, *Soft Matter* **2022**, *18*, 5535–5561.
[58] S. W. Kuo, *J. Polym. Res.* **2022**, *29*, 69.
[59] T. C. Tseng, S. W. Kuo, *Macromolecules* **2018**, *51*, 6451–6459.
[60] S. W. Kuo, C. L. Lin, F. C. Chang, *Polymer* **2002**, *43*, 3943–3949.
[61] M. Ejaz, M. M. Samy, Y. Ye, S. W. Kuo, M. G. Mohamed, *Int. J. Mol. Sci.* **2023**, *24*, 2501.
[62] M. G. Mohamed, M. H. Elsayed, Y. Ye, M. M. Samy, A. E. Hassan, T. H. Mansoure, Z. Wen, H. H. Chou, K. H. Chen, S. W. Kuo, *Polymer* **2023**, *15*, 182.
[63] M. M. Samy, M. G. Mohamed, S. U. Sharma, S. V. Chaganti, T. H. Mansoure, J. T. Lee, T. Chen, S. W. Kuo, *Polymer* **2023**, *264*, 125541.
[64] W. Lyu, C. Yan, Z. Chen, J. Chen, H. Zuo, L. Teng, H. Liu, L. Wang, Y. Liao, *ACS Appl. Energ. Mater.* **2022**, *5*, 3706–3714.
[65] M. Ejaz, M. G. Mohamed, S. U. Sharma, J. T. Lee, C. F. Huang, T. Chen, S. W. Kuo, *Molecules* **2022**, *27*, 6238.
[66] M. G. Mohamed, H. Y. Hu, M. Madhu, M. M. Samy, I. M. A. Mekhemer, W. L. Tseng, H. H. Chou, S. W. Kuo, *Eur. Polym. J.* **2023**, *189*, 111980.
[67] M. M. Samy, M. G. Mohamed, S. W. Kuo, *Polymer* **2023**, *15*, 1095.
[68] M. M. Samy, M. G. Mohamed, S. U. Sharma, S. V. Chaganti, J. T. Lee, S. W. Kuo, *J. Taiwan Inst. Chem. Eng.* **2023**, 104750.

Manuscript received: February 18, 2023
Accepted manuscript online: March 18, 2023
Version of record online: April 19, 2023